Z. Phys. C – Particles and Fields 44, 415–432 (1989)

Zeitschrift für Physik C Particles and Fields

QCD Jets at HERA

II. $O(\alpha_s^2)$ four-jet cross-sections

T. Brodkorb[1], J.G. Körner[1], E. Mirkes[1], G.A. Schuler[2]

[1] Institut für Physik, Johannes Gutenberg-Universität, D-6500 Mainz, Federal Republic of Germany
[2] II. Institut für Theoretische Physik, Universität, D-2000 Hamburg 50, Federal Republic of Germany

Received 7 March 1989

Abstract. We present exact expressions for the $O(\alpha_s^2)$ tree graph four-jet cross-sections in neutral current and charged current deep inelastic *ep* scattering initiated by quarks, antiquarks and gluons including lepton polarization effects. Using helicity amplitudes the partonic cross-sections are given in concise form including all colour, flavour and statistical factors. We explicate the electroweak coupling dependence and state how the partonic cross-sections are folded with the respective parton densities to obtain the *ep* jet cross-sections to $O(\alpha_s^2)$. We present some numerical results for the neutral current one-photon exchange case. We elaborate on the cut dependence of the jet rates and present differential distributions in some basic kinematical variables.

1 Introduction

With the study of very high energy lepton-proton collisions possible at HERA ($\sqrt{s} \simeq 314\,\text{GeV}$) final states consisting of multiple parton jets will be abundant [1]. Jet production rates and their comparison with perturbative QCD will constitute an important part of the physics program at HERA. Also, there is a need to accurately asses production rates and characteristics of QCD-originated jets since they will be an important background to possible rare and exotic physics processes at HERA.

To this end one needs the exact perturbative QCD cross-sections for multiparton processes initiated by quark, antiquark and gluon partons in the proton. To $O(\alpha_s)$ one has 3-jet final states*. The necessary $O(\alpha_s)$ cross-section formulae are well documented in [2–5]. Predictions for higher multiplicity jet rates exist only in form of parton cascade models (see e.g. [6]) that account only for the leading behaviour of the exact perturbative QCD matrix elements [7, 8]. As one will progress to look more closely at the details of multiple jet production one needs to be able to avail of the exact higher order QCD matrix elements.

It is the purpose of this paper to provide the exact $O(\alpha_s^2)$ 4-jet-production cross-sections in neutral current (NC) and charged current (CC) deep inelastic scattering (DIS) initiated by quark, antiquark and gluon partons including initial lepton polarization effects.

We compute the $O(\alpha_s^2)$ partonic hard scattering cross-sections by first evaluating all the helicity amplitudes of the basic parton processes where we treat the partons as massless. This has numerous advantages. First, by using the new elegant helicity techniques together with their clever gauge choices introduced in [9–12] one arrives at very compact expressions for the helicity amplitudes despite of the many Feynman diagrams that contribute to each basic scattering process. To be specific, we calculate the helicity amplitudes using the Weyl-van der Waerden formalism which was introduced in [13] and [14] and further developed in [15]. The complex-valued helicity amplitudes are evaluated numerically. This procedure leads to a very simple and efficient way of numerically evaluating cross-section values by calculating the cross-section as sum of square moduli of the numerically evaluated helicity amplitudes. Finally, polarisation type effects can be calculated quite easily once the helicity amplitudes of the process are known. The DIS cross-sections can then be obtained from the partonic hard scattering cross-sections by folding in the relevant partonic distribution functions as usual as depicted in Fig. 1.

In Sect. 2 we calculate the helicity amplitudes for all parton scattering processes $l + p \to l' + p_1 + p_2 + p_3$ where l and l' are the momenta of the initial and final leptons, and p is the initial parton and p_1, p_2, p_3 are the final partons. We briefly recapitulate some of the basic notions of the Weyl-van der Waerden helicity formalism as introduced in [15]. This is necessary to

* We include the target jet when counting the number of produced jets

guide the reader through the calculation as well as to define some basic notation of the formalism that appear in the final formulae. We write down a minimal set of vector current-induced hard scattering helicity amplitudes for the two quark-two gluon case and the four-quark case. We specify how the remaining helicity amplitudes are related to the minimal set by parity, charge conjugation and crossing. Simple rules are given that relate the axial vector current-induced helicity amplitudes to the corresponding vector current amplitudes. We also specify the numerical procedure that is used to evaluate the helicity amplitudes numerically.

In Sect. 3 we provide the material necessary to calculate the partonic cross-sections from the helicity amplitudes, i.e. we write down the necessary colour, flavour and statistical factors that are needed to obtain the partonic cross-section from the squared moduli of the helicity amplitudes. We also write down the basic parity-violating (pv) and parity-conserving (pc) flavour couplings of the standard model for the NC and CC case and specify how they multiply the helicity amplitudes. After squaring and summing the helicity amplitudes one obtains the characteristic electroweak flavour coupling combinations multiplying the pc and pv DIS cross-sections that one is familiar with in the corresponding $O(\alpha_s^0)$ and $O(\alpha_s)$ cases (see e.g. [5]). In exception is the four-quark case which is more involved due to interference contributions where the electroweak currents couple to different quark lines. These lead to nondiagonal flavour coupling terms on the one hand and to a new flavour structure due to an explicit breaking of γ^5-invariance on the other hand. The resulting new pc and pv electroweak flavour structure for the interference terms is fully specified.

In Sect. 4 we introduce the $2 \to 4$ electroproduction phase space relevant for the hard parton scattering process $l + p \to l' + p_1 + p_2 + p_3$. We then specify how the partonic hard scattering cross-sections are folded with the respective parton densities to obtain the DIS 4-jet cross-section. Section 5 contains our numerical results where we have decided to limit our discussion to the pure NC one-photon exchange case*. We discuss overall kinematical cuts that we choose to define our DIS electroproduction phase space. Further cuts are then imposed on the invariant jet-jet masses, s_{ij}, to define the resolved 4-jet phase space. These cuts serve to exclude the IR (infrared)/M (mass or collinear) singular regions where the 4-jet cross-section diverges. We present predictions on 4-jet rates and compare them to 3-jet rates and the total DIS cross-section. The respective jet rates are given as functions of various cut parameters, and as functions of the overall CM energy s, and the kinematical variables x, y and W^2. Section 6, finally, contains our summary and the conclusions.

* We hope to return to a more detailed numerical discussion including Z- and W-exchange effects in a future publication

We would like to mention that this paper is the second one in a series of papers devoted to the study of QCD jet production effects in leptoproduction. In the first paper of the series [5] we have discussed the complete $O(\alpha_s)$ corrections to the electroweak 2-jet cross-sections of both neutral and charged current scattering including lepton polarization effects. It also contains an extended discussion of the problems of how to define jet cross-sections in eP-scattering. In the third paper of this series we shall discuss the $O(\alpha_s^2)$ radiative corrections to 3-jet production rates in DIS.

2 Evaluation of helicity amplitudes in the Weyl-van der Waerden formalism

2.1 Basic notions of the Weyl-van der Waerden formalism

The first step in evaluating helicity amplitudes in the Weyl-van der Waerden formalism is to replace spinors, γ-matrices, etc. in the usual covariant Feynman amplitude representation by their Weyl-van der Waerden two-spinor counterparts. In the following we write down the necessary replacements where we follow the conventions of [15]. We remind the reader that we take all partons and leptons as massless.

1. helicity spinors

$$\begin{aligned} u_+(P) &= v_-(P) \to p_B \\ u_-(P) &= v_+(P) \to p^{\dot{B}} \\ \bar{u}_+(Q) &= \bar{v}_-(Q) \to -iq_{\dot{A}} \\ \bar{u}_-(Q) &= \bar{v}_+(Q) \to iq^A \end{aligned} \tag{1}$$

   where the subscripts $\pm$ on the spinors refer to the helicities of the respective fermions.

2. γ-matrices, momenta and polarization vectors slashed

$$\gamma^\mu \to i\sigma^{\mu\dot{A}B} - i\sigma^\mu_{BA} \tag{2}$$

$$\not{K} \to ik^{\dot{A}}k^B - ik_B k_A \quad \text{where } K^2 = 0 \tag{3}$$

$$\not{\epsilon}^*_+(K) \to \frac{\sqrt{2}}{\langle kg \rangle}(ik_{\dot{B}}g_A - ik^{\dot{A}}g^B) \tag{4}$$

$$\not{\epsilon}^*_-(K) \to \frac{\sqrt{2}}{\langle kg \rangle^*}(ig_{\dot{B}}k_A - ig^{\dot{A}}k^B), \tag{5}$$

where g is a gauge spinor related to any four-momentum which can be conveniently specified. Note that we normalize our polarization vectors to (-1). This normalisation differs from the one used in [15]. Polarization four-vectors can also occur in an "unslashed" form due to the three-gluon coupling. These can be transcribed to the above "slashed" polarization four-vectors by using the identity

$$2\varepsilon_\mu I = \gamma_\mu \not{\epsilon} + \not{\epsilon}\gamma_\mu.$$

We use upper case letters for massless four-momentum vectors and lower case letters for the

"momentum" spinors associated with them. This suggestive notation was introduced in [15]. The momentum spinors are in some sense "square roots" of the four-momenta associated with them. We caution the reader that we use this suggestive notation *only* in this section where the helicity amplitudes are calculated. In later sections we freely dispose of upper case and lower case momenta without the momentum spinor identification in the latter case.

The dotted and undotted upper and lower indices take the values 1 and 2. Tensor contractions are to be done only for upper-lower pairs of dotted (undotted) indices, where a summation over repeated indices is understood. Terms that cannot be summed in this sense have to be dropped.

A contraction of 2 two-spinors associated with massless particles can be viewed as a complex-valued scalar-product and will be referred to as a spinor-inner-product.

$$p_A q^A = \langle pq \rangle, \tag{6}$$

If one sums over dotted instead of undotted indices one gets the complex-conjugate of the same spinor-inner-product, i.e.

$$p_{\dot{A}} q^{\dot{A}} = \langle pq \rangle^*. \tag{7}$$

Spinors with upper and lower indices are related by means of the two-dimensional antisymmetric "metric tensor",

$$\varepsilon^{AB} = \varepsilon_{\dot{A}\dot{B}} = -\varepsilon_{AB} = -\varepsilon^{\dot{A}\dot{B}} = \begin{pmatrix} 0 & 1 \\ -1 & 0 \end{pmatrix} \tag{8}$$

via

$$p^A \varepsilon_{AB} = p_B \tag{9}$$

$$p_{\dot{A}} \varepsilon^{\dot{A}\dot{B}} = p^{\dot{B}}. \tag{10}$$

This leads to the relation

$$\langle pq \rangle = -\langle qp \rangle. \tag{11}$$

One has to be very careful with the position and type of indices. Thus one has e.g. $\varepsilon_{BA} p^A = -p_B$. In the evaluation of helicity amplitudes one makes use of the following important identities:

1. Scalar four product

$$\langle pq \rangle \langle pq \rangle^* = 2PQ \tag{12}$$

2. Schouten identities

$$\varepsilon^{AB}\varepsilon^{CD} + \varepsilon^{AC}\varepsilon^{DB} + \varepsilon^{AD}\varepsilon^{BC} = 0 \tag{13}$$

$$\varepsilon^{\dot{A}\dot{B}}\varepsilon^{\dot{C}\dot{D}} + \varepsilon^{\dot{A}\dot{C}}\varepsilon^{\dot{D}\dot{B}} + \varepsilon^{\dot{A}\dot{D}}\varepsilon^{\dot{B}\dot{C}} = 0 \tag{14}$$

3. Anticommutator of γ-matrices

$$\sigma^{\mu}_{A\dot{B}}\sigma^{\nu\dot{C}B} + \sigma^{\nu}_{A\dot{B}}\sigma^{\mu\dot{C}B} = 2g^{\mu\nu}\delta^{\dot{C}}_{\dot{A}} \tag{15}$$

$$\sigma^{\mu\dot{B}A}\sigma^{\nu}_{B\dot{C}} + \sigma^{\nu\dot{B}A}\sigma^{\mu}_{B\dot{C}} = 2g^{\mu\nu}\delta^{A}_{C} \tag{16}$$

4. Fierz-transformations

$$\sigma^{\mu\dot{A}B}\sigma_{\mu}^{\dot{C}D} = 2\varepsilon^{\dot{A}\dot{C}}\varepsilon^{BD} \tag{17}$$

$$\sigma^{\mu\dot{A}B}\sigma_{\mu\dot{C}D} = 2\delta^{\dot{A}}_{\dot{C}}\delta^{B}_{D} \tag{18}$$

$$\sigma^{\mu}_{A\dot{B}}\sigma_{\mu\dot{C}D} = 2\varepsilon_{\dot{A}\dot{C}}\varepsilon_{BD}. \tag{19}$$

A very important ingredient to obtain compact expressions for the helicity amplitudes from the Feynman amplitudes is the choice of an optimal gauge, i.e. the choice of the gauge spinors g in (4) and (5). The optimal choice of gauge may in fact even depend on the specific helicity amplitude that is being calculated. This becomes relevant for the two quark-two gluon ($qqgg$) process to be discussed in the following. In these processes the optimal choice is to use one of the momenta of the quark to which the two gluons are coupled as a gauge spinor. It turns out that with such an optimal choice only 5 of the 8 contributing Feynman graph amplitudes contribute for any given helicity configuration.

2.2 Results for helicity amplitudes

There are two classes of contributions to the $2 \to 4$ parton process $l + p \to l' + p_1 + p_2 + p_3$. These are the processes involving two quarks and two gluons ($qqgg$) and the processes involving four quarks ($qqqq$). The results for the corresponding helicity amplitudes will be presented in turn. Four-momenta will be denoted by upper case letters and the momentum spinors associated with them by lower case letters. We emphasize again that this distinction will not be followed through in Sects. 3, 4 and 5 since there is no explicit mention of momentum spinors in the later sections.

i) Two quark-two gluon processes ($qqgg$). The two quark-two gluon processes relevant for DIS are

$$l + q \to l' + q + g + g \tag{20}$$

$$l + \bar{q} \to l' + \bar{q} + g + g \tag{21}$$

$$l + g \to l' + q + \bar{q} + g. \tag{22}$$

A representative Feynman diagram contribution for each of the above processes has been drawn in Fig. 1.

Clearly there are $2^4 = 16$ nonvanishing helicity amplitudes involved in these processes, since the gluon helicities can take the two values $\{\pm 1\}$ whereas, due to helicity conservation, the fermion helicities can take the values $\{\pm 1/2\}$ for each fermionic pair of leptons and quarks only. However, it suffices to write down only two of the 16 helicity amplitudes. The other 14 helicity amplitudes can then be obtained from parity, charge conjugation and crossing as will be shown later on.

It turns out that there are basically two types of helicity amplitudes, namely those with equal gluon helicities and those with different gluon helicities. When one has equal gluon helicities the helicity amplitudes simplify as one can cancel many propagators. The result is a very compact final expression.

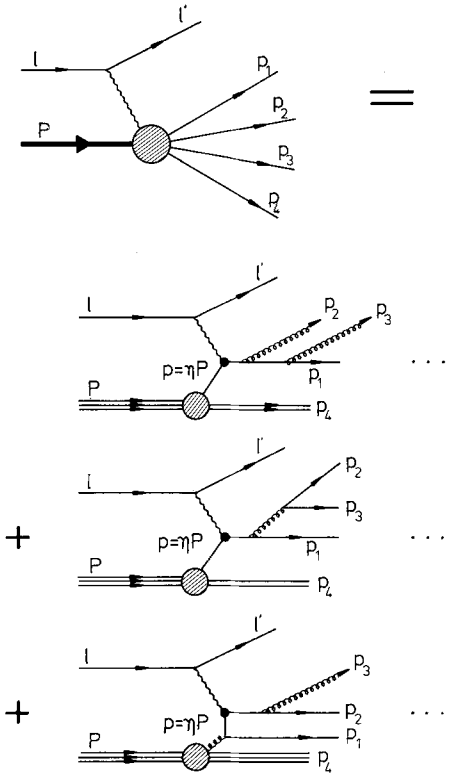

Fig. 1. Generic diagram of 4-jet production in deep inelastic ep scattering. Also shown are examples of the three $O(\alpha_s^2)$ processes contributing to 4-jet events. The proton remnant is counted as a separate jet

The case of unequal gluon helicities is more involved and does not reduce to a very simple expression.

We write down our results for the case of the quark initiated process (20). Later on we specify the crossing rules that allow one to read off the corresponding expressions for antiquark (21) and gluon initiated processes (22). Further we start our discussion with purely parity conserving amplitudes corresponding to vector current coupling at both the leptonic and hadronic vertices as is relevant for the usual one-photon exchange case. Axial vector current couplings will be discussed later on.

Each of the partons will be labelled by its helicity, momentum and colour. Thus one has

$$l(\lambda_L, L) + q(\lambda_0, P, i) \to l'(\lambda_{L'}, L') + q(\lambda_1, P_1, j) + g(\lambda_2, P_2, a) + g(\lambda_3, P_3, b), \tag{23}$$

where i and j and a and b are colour indices of the quarks ($i,j = 1 \cdots 3$) and gluons ($a,b = 1 \cdots 8$) respectively. The helicities of the leptons and partons are denoted by λ. The L, L' and P, P_i are the four-momenta of the leptons and partons, respectively. For the corresponding helicity amplitudes we write:

$$h^{vV}_{q\to qgg}(\lambda_0, P, i; \lambda_1, P_1, j; \lambda_2, P_2, a; \lambda_3, P_3, b; \lambda_L, L; \lambda_{L'}, L')$$

where the lower case v stands for the vector current at the leptonic vertex and the upper case V stands for the vector current at the hadronic vertex. In order to keep our notation reasonably concise, we shall always drop those quantum number labels that are not important for the argument at hand.

Equal gluon helicities:

$$h^{vV}_{q\to qgg}(+;+;+;+;+;+) = 2ie^2g^2\frac{\langle lp\rangle^2}{\langle ll'\rangle} \cdot\left\{\frac{T^aT^b}{\langle p_1p_2\rangle\langle p_2p_3\rangle\langle p_3p\rangle} + \frac{T^bT^a}{\langle p_1p_3\rangle\langle p_3p_2\rangle\langle p_2p\rangle}\right\} \tag{24}$$

Opposite gluon helicities:

$$\begin{aligned} &h^{vV}_{q\to qgg}(+;+;-;+;+;+) \\ &= \frac{ie^2g^2}{(LL')(P_2P_3)\langle pp_3\rangle\langle p_1p_2\rangle^*\langle p_1p_3\rangle\langle pp_2\rangle^*} \\ &\cdot\{-T^bT^a(P_2P_3)(\langle lp\rangle\langle ll'\rangle^* - \langle p_2p\rangle\langle p_2l'\rangle^*) \\ &\cdot(\langle l'l\rangle\langle l'p_1\rangle^* + \langle p_3l\rangle\langle p_3p_1\rangle^*) \\ &- \frac{T^aT^b(P_1P_3) - T^bT^a(P_1P_3 + P_2P_3)}{(P_1+P_2+P_3)^2} \\ &\cdot\langle p_1p_3\rangle^*\langle pl\rangle\langle pp_2\rangle^*\langle pp_3\rangle \\ &\cdot(\langle ll'\rangle^*\langle lp_2\rangle + \langle pl'\rangle^*\langle pp_2\rangle) \\ &+ \frac{T^aT^b(PP_2) - T^bT^a(PP_2 - P_2P_3)}{(-P+P_2+P_3)^2} \\ &\cdot\langle p_1l'\rangle^*\langle pp_2\rangle\langle p_1p_2\rangle\langle p_1p_3\rangle \\ &\cdot(\langle l'l\rangle\langle l'p_3\rangle^* + \langle p_1l\rangle\langle p_1p_3\rangle^*) \\ &+ 2(T^aT^b - T^bT^a)(P_1P_3)(PP_2)\langle p_1l'\rangle^*\langle pl\rangle\}, \end{aligned} \tag{25}$$

where e and g are the electromagnetic and the strong QCD coupling constants, respectively ($e^2/4\pi = \alpha$ and $g^2/4\pi = \alpha_s$). The appropriate coupling factors of quarks and leptons to the γ and $Z^0(W^\pm)$ and the appropriate propagator factor modifications due to $Z^0(W^\pm)$ exchange will be added later on. In order to save on notation we have dropped the spin label on the helicity labels in (24, 25). Thus $(\pm)$ means $(\pm\frac{1}{2})$ in the case of leptons and quark helicities, and (± 1) in the case of gluon helicities, respectively.

As mentioned above the remaining 14 helicity amplitudes can be obtained from the two helicity amplitudes (24, 25) by parity, charge conjugation and crossing. From CP invariance one has:

$$h^{vV}(\lambda_0;\lambda_1;\lambda_2;\lambda_3;\lambda_L;\lambda_{L'}) = (h^{vV}(-\lambda_0;-\lambda_1;-\lambda_2;-\lambda_3;-\lambda_L;-\lambda_{L'}))^*. \tag{26}$$

The remaining six helicity amplitudes are obtained from crossing:

$$h^{vV}_{q\to qgg}(\lambda_0;\lambda_1;\lambda_2;\lambda_3;-\lambda_L,L;-\lambda_{L'},L') = -h^{vV}_{q\to qgg}(\lambda_0;\lambda_1;\lambda_2;\lambda_3;\lambda_L,-L';\lambda_{L'},-L) \tag{27}$$

$$h^{vV}_{q\to qgg}(-,P;-,P_1;\lambda_2,a;\lambda_3,b;\lambda_L;\lambda_{L'}) = -h^{vV}_{q\to qgg}(+,-P_1;+,-P;\lambda_2,b;\lambda_3,a;\lambda_L;\lambda_{L'}). \tag{28}$$

In order to give a meaning to the crossing relations (27, 28) one has to define spinor inner products with negative momentum spinor components. A discussion of this point is delayed to the end of Sect. 2.5 where we specify our numerical procedure to evaluate the helicity amplitudes. Finally, when both lepton- and quark-helicities are reversed one uses both (27, 28).

The phase choice taken in Sect. 2.5 (46) for spinor inner products with negative momentum spinor components is compensated for in (27, 28) by multiplying an extra minus sign. The resulting phases of the helicity amplitudes are the phases that would result from an explicit ab initio calculation of the remaining helicity amplitudes using the explicit spinor and polarisation vector representation written down in (1, 4, 5).

ii) Four-quark processes (qqqq). The four-quark processes relevant for DIS are (see Fig. 1)

$$l+q\to l'+q+q+\bar{q} \tag{29}$$

$$l+\bar{q}\to l'+\bar{q}+\bar{q}+q. \tag{30}$$

For these four-quark processes one has to take into account that one has the two possibilities that all quark flavours are equal and that one has two different pairs of quark flavours. The latter case is simpler since the number of contributing Feynman diagrams is reduced by a factor two from eight to four. However, it is simpler to discuss the two cases of equal and unequal quark flavours concurrently. The simplifications that occur in the unequal flavour case will be obvious from the structure of the following equations. One considers the following process:

$$\begin{aligned} &l(\lambda_L,L)+q_f(\lambda_0,P,i)\to l'(\lambda_{L'},L')+q_f(\lambda_1,P_1,j)\\ &\quad+q_{f'}(\lambda_2,P_2,k)+\bar{q}_{f'}(\lambda_3,P_3,l). \end{aligned} \tag{31}$$

Within this equation i,j,k and l are colour indices of the four quarks. For the helicity amplitudes we write:

$$\begin{aligned} &h^{vV}_{q_f\to q_f q_{f'}\bar{q}_{f'}}\\ &\cdot(\lambda_0,P,i;\lambda_1,P_1,j;\lambda_2,P_2,k;\lambda_3,P_3,l;\lambda_L,L;\lambda_{L'},L'). \end{aligned}$$

Due to the necessary antisymmetrization in the equal flavour case ($f=f'$) there are twelve nonvanishing helicity amplitudes in the equal flavour case ($f=f'$), whereas there are only eight helicity amplitudes in the unequal flavour case ($f\neq f'$).

In the four-quark case there is no "optimal" choice of the gauge spinor g as in the two quark-two gluon case that would lead to the dramatic simplifications encountered in the latter case. Obviously the helicity formalism in this process leaves no choice of a gauge for each helicity configuration. Therefore all Feynman diagrams contribute to each helicity amplitude. For later purposes it is convenient to keep track which Feynman diagram contributes to which term in the various expressions of the helicity amplitudes. To this end we have drawn the eight contributing Feynman diagrams in Fig. 2 and numbered them from 1 to 8. The corresponding contributions can be identified in the following expressions for the helicity amplitudes by the coefficients a_i $(i=1,\ldots,8)$.

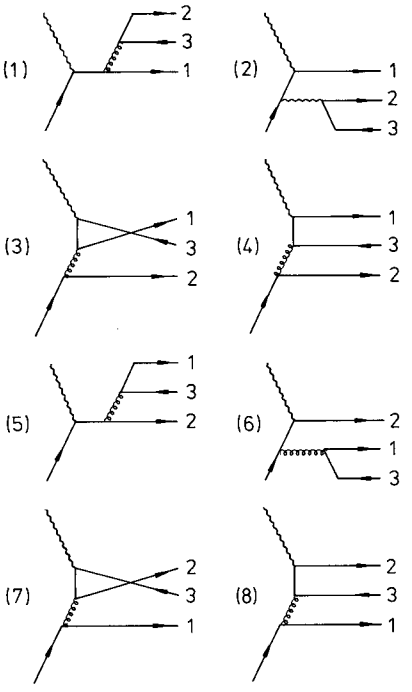

Fig. 2. The eight $O(\alpha_s^2)$ diagrams contributing to the process (boson $+\,q_f\to q_f+q_{f'}+\bar{q}_{f'}$)

One has

$$\begin{aligned} &h^{vV}_{q\to qq\bar{q}}(+;+;+;-;+;+)\\ &=\frac{-ie^2g^2}{LL'}\Bigg\{-\left(a_7\frac{1}{PP_1}T^a_{ij}T^a_{kl}+a_3\frac{1}{PP_2}T^a_{il}T^a_{kj}\right)\\ &\quad\cdot\langle p_3 l\rangle\langle p_2p_1\rangle^*(-P+P_1+P_2)^{-2}\\ &\quad\cdot(\langle ll'\rangle^*\langle lp\rangle-\langle p_3l'\rangle^*\langle p_3p\rangle)\\ &\quad-\left(a_1\frac{1}{P_2P_3}T^a_{ij}T^a_{kl}+a_5\frac{1}{P_1P_3}T^a_{il}T^a_{kj}\right)\\ &\quad\cdot\langle pl\rangle\langle p_2p_1\rangle^*(P_1+P_2+P_3)^{-2}\\ &\quad\cdot(\langle ll'\rangle^*\langle lp_3\rangle+\langle pl'\rangle^*\langle pp_3\rangle)\\ &\quad+\left(a_2\frac{1}{P_2P_3}T^a_{ij}T^a_{kl}-a_4\frac{1}{PP_2}T^a_{il}T^a_{kj}\right)\\ &\quad\cdot\langle pp_3\rangle\langle p_1l'\rangle^*(-P+P_2+P_3)^{-2}\\ &\quad\cdot(\langle l'l\rangle\langle l'p_2\rangle^*+\langle p_1l\rangle\langle p_1p_2\rangle^*)\\ &\quad+\left(a_8\frac{1}{PP_1}T^a_{ij}T^a_{kl}-a_6\frac{1}{P_1P_3}T^a_{il}T^a_{kj}\right)\\ &\quad\cdot\langle pp_3\rangle\langle p_2l'\rangle^*(-P+P_1+P_3)^{-2}\\ &\quad\cdot(\langle l'l\rangle\langle l'p_1\rangle^*+\langle p_2l\rangle\langle p_2p_1\rangle^*)\Bigg\} \end{aligned} \tag{32}$$

$$h^{vV}_{q\to qq\bar{q}}(+;+;-;+;+;+)$$
$$=\frac{-ie^2g^2}{LL'}T^a_{ij}T^a_{kl}\Big[a_1\frac{1}{P_2P_3}\langle pl\rangle\langle p_1p_3\rangle^*$$
$$\cdot(P_1+P_2+P_3)^{-2}(\langle ll'\rangle^*\langle lp_2\rangle+\langle pl'\rangle^*\langle pp_2\rangle)$$
$$+a_7\frac{1}{PP_1}\langle pp_2\rangle\langle l'p_3\rangle^*(-P+P_1+P_2)^{-2}$$
$$\cdot(\langle l'l\rangle\langle l'p_1\rangle^*+\langle p_3l\rangle\langle p_3p_1\rangle^*)$$
$$+a_2\frac{1}{P_2P_3}\langle pp_2\rangle\langle p_1l'\rangle^*(-P+P_2+P_3)^{-2}$$
$$\cdot(\langle l'l\rangle\langle l'p_3\rangle^*+\langle p_1l\rangle\langle p_1p_3\rangle^*)$$
$$-a_8\frac{1}{PP_1}\langle p_2l\rangle\langle p_1p_3\rangle^*(-P+P_1+P_3)^{-2}$$
$$\cdot(\langle ll'\rangle^*\langle lp\rangle-\langle p_2l'\rangle^*\langle p_2p\rangle)\Big] \tag{33}$$

$$h^{vV}_{q\to qq\bar{q}}(-;+;-;-;+;+)$$
$$=\frac{-ie^2g^2}{LL'}T^a_{il}T^a_{kj}\Big[a_5\frac{1}{P_1P_3}\langle p_2p_3\rangle\langle pl'\rangle^*$$
$$\cdot(P_1+P_2+P_3)^{-2}(\langle l'p_1\rangle^*\langle l'l\rangle-\langle pp_1\rangle^*\langle pl\rangle)$$
$$+a_3\frac{1}{PP_2}\langle lp_3\rangle\langle pp_1\rangle^*(-P+P_1+P_2)^{-2}$$
$$\cdot(\langle ll'\rangle^*\langle lp_2\rangle-\langle p_3l'\rangle^*\langle p_3p_2\rangle)$$
$$-a_6\frac{1}{P_1P_3}\langle lp_2\rangle\langle pp_1\rangle^*(-P+P_1+P_3)^{-2}$$
$$\cdot(\langle ll'\rangle^*\langle lp_3\rangle-\langle p_2l'\rangle^*\langle p_2p_3\rangle)$$
$$-a_4\frac{1}{PP_2}\langle p_2p_3\rangle\langle p_1l'\rangle^*(-P+P_2+P_3)^{-2}$$
$$\cdot(\langle l'p\rangle^*\langle l'l\rangle+\langle p_1p\rangle^*\langle p_1l\rangle)\Big]. \tag{34}$$

The remaining nine nonvanishing helicity amplitudes can again be obtained from the above three by applying parity, charge conjugation and crossing according to the rules written down in (26, 27). Note, though, that (28) is not valid in the four-quark case since the fermion line initiated by the quark with momentum P can connect to a final quark with either momentum P_1 or P_2. As mentioned above the suffix i in the coefficients a_i identifies the contributing Feynman diagram. These coefficients take the values ±1 and 0 as specified in Table 1.

It is clear from the structure of (32, 33, 34) that there are altogether only eight nonvanishing helicity amplitudes in the unequal flavour case ($f\neq f'$) as stated above. The diagrams ($i=3, 4, 5, 6$) consist of fermion lines connecting a quark with flavour f to a quark with flavour f' (see Fig. 2). For $f\neq f'$ these contributions vanish, i.e. the helicity amplitude (34) vanishes. Also the three helicity amplitudes that would be derived from (34) with the help of (26, 27) vanish.

2.3 *Axial vector current helicity amplitudes*

When one wants to investigate also party-violating (pv) effects in DIS one needs the axial vector current helicity amplitudes also. This involves the replacement of the vector current by the axial vector current at either or both the leptonic and hadronic vertices. This replacement is effected by

$$\gamma^\mu\to\gamma^\mu\gamma^5 \tag{35}$$

at the leptonic and/or hadronic current vertex. In terms of the Weyl–van der Waerden representation this implies the replacement

$$i\sigma^{\mu\dot{A}B}-i\sigma^{\mu}_{BA}\to i\sigma^{\mu\dot{A}B}+i\sigma^{\mu}_{BA}\,. \tag{36}$$

Thus the helicity amplitudes change sign every time a term σ^μ contributes with lowered spinor indices. This will depend on the fermionic lepton and quark helicities.

For the leptonic vertex one then obtains the relation

$$h^{aV}=(-)^{1/2-\lambda_L}h^{vV} \tag{37}$$

and the same for $V\to A$. Relation (37) is true irrespective of the associated parton process.

An analogous relation holds true when one replaces the hadronic vector current by the axial hadronic vector current, i.e. $V\leftrightarrow A$ in the two quark-two gluon processes.

$$h^{vA}_{q\to qgg}=(-)^{1/2-\lambda_1}h^{vV}_{q\to qgg} \tag{38}$$

Table 1. Feynman diagram factors a_i for processes involving four quarks (four-quark case)

Helicity amplitudes	Hadronic vector current $h^{vV}_{q\to qq\bar{q}}$		Hadronic axial vector current $h^{vA}_{q\to qq\bar{q}}$	
$+++-++$	$a_i=1,\ i=1,\ldots,8$	$f=f'$	$a_i=1,\ i=1,\ldots,8$	$f=f'$
	$a_j=1,\ j=1,2,7,8$ $a_j=0,\ j=3,4,5,6$	$f\neq f'$	$a_j=1,\ j=1,2,7,8$ $a_j=0,\ j=3,4,5,6$	$f\neq f'$
$++-+++$	$a_i=1,\ i=1,\ldots,8$	$f=f'$	$a_i=+1,\ i=5,6,7,8$ $a_i=-1,\ i=1,2,3,4$	$f=f'$
$-+--++$	$a_j=1,\ j=1,2,7,8$ $a_j=0,\ j=3,4,5,6$	$f\neq f'$	$a_i=+1,\ i=7,8$ $a_i=-1,\ i=1,2$ $a_i=0,\ i=3,4,5,6$	$f\neq f'$

No such simple rule exists for the four-quark processes due to the fact that the hadronic axial vector coupling can occur at either of the two quark lines. At one-half of the Feynman diagrams the electroweak currents couple to the quark-line which is associated with the quark-helicity λ_1. This is the case for the Feynman diagrams $i = 1, 2, 3, 4$ (see Fig. 2). For these terms one has the same relation (38) as in the two quark-two gluon case, namely

$$(1,2,3,4): \quad h^{vA}_{q\to qq\bar{q}} = (-)^{1/2-\lambda_1} h^{vV}_{q\to qq\bar{q}}. \tag{39}$$

At the other half of Feynman diagrams the electroweak currents couple to the quark-line associated with the quark-helicity λ_2. (Feynman diagrams $i = 5, 6, 7, 8$). For these contributions one finds

$$(5,6,7,8): \quad h^{vA}_{q\to qq\bar{q}} = (-)^{1/2-\lambda_2} h^{vV}_{q\to qq\bar{q}}. \tag{40}$$

Relations (38, 39, 40) hold true irrespective of the coupling at the leptonic side, i.e. when interchanging $v \leftrightarrow a$.

In the unequal helicity case $\lambda_1 \neq \lambda_2$ note that $h^{vA}_{q\to qq\bar{q}} \neq \pm h^{vV}_{q\to qq\bar{q}}$ since one-half of the contributions within a helicity amplitude change sign whereas the other half does not. This is clear evidence for the breaking of γ^5-invariance in the four-quark processes*. We will have to return to the breaking of γ^5-invariance when we discuss cross-sections.

2.4 *Helicity amplitudes for antiquark and gluon initiated processes*

Up to this point we have concentrated on calculating the helicity amplitudes for quark-initiated hard scattering processes. Within the parton model approach one has in addition also contributions from gluon and antiquark initiated processes. The relevant helicity amplitudes can be obtained from the quark initiated helicity amplitudes through crossing. One has

$$\begin{aligned} &h_{\bar{q}\to\bar{q}gg}(\lambda_0, P, i; \lambda_1, P_1, j; \lambda_2, a; \lambda_3, b; \lambda_L; \lambda_{L'}) \\ &\quad = -h_{q\to qgg}(-\lambda_1, -P_1, j; -\lambda_0, \\ &\qquad -P, i; \lambda_2, b; \lambda_3, a; \lambda_L; \lambda_{L'}) \end{aligned} \tag{41}$$

$$\begin{aligned} &h_{g\to q\bar{q}q}(\lambda_0, P, a; \lambda_1; \lambda_2, P_2, j; \lambda_3; \lambda_L; \lambda_{L'}) \\ &\quad = -h_{q\to qgg}(-\lambda_2, -P_2, j; \lambda_1; -\lambda_0, \\ &\qquad -P, a; \lambda_3; \lambda_L; \lambda_{L'}) \end{aligned} \tag{42}$$

$$\begin{aligned} &h_{\bar{q}\to\bar{q}q\bar{q}}(\lambda_0, P, i; \lambda_1, P_1, j; \lambda_2, P_2; \lambda_3, P_3; \lambda_L; \lambda_{L'}) \\ &\quad = -h_{q\to qq\bar{q}}(-\lambda_1, -P_1, j; -\lambda_0, \\ &\qquad -P, i; \lambda_3, P_3; \lambda_2, P_2; \lambda_L; \lambda_{L'}). \end{aligned} \tag{43}$$

The implementation of these crossing rules in terms of spinor inner products involving negative four-momenta is discussed in (46). We emphasize that it is very important to accurately keep track of the order of colour indices in the crossing relations (41–43). Since the crossing properties do not depend on the vector or axial vector coupling properties of the helicity amplitudes we have dropped the relevant superscripts.

2.5 *Numerical procedure for the evaluation of spinor-inner-products*

If one attempts to compute the squared moduli of the helicity amplitudes analytically by using e.g. the algorithm given in [15] one encounters traces with up to twelve momenta slashed*. We have checked that the resulting analytical expressions are comparable in length to those obtained by the conventional covariant ("sum and square") method. One therefore looses the advantages of the compactness of the helicity amplitude expressions. However, one can maintain compactness (and therefore possibly speed) by evaluating the helicity amplitudes numerically and then obtain their squared moduli numerically.

We use the following procedure. First, one chooses a definite representation for the two-spinors. Within such a definite representation one can then evaluate the spinor-inner-products numerically. With the choice of spinors made by [15] one obtains the following representation for the complex-valued spinor-inner-product:

$$\begin{aligned} \langle kp \rangle = &\sqrt{(K_0 + K_3)(P_0 - P_3)}\, e^{i\varphi(K)} \\ &- \sqrt{(P_0 + P_3)(K_0 - K_3)}\, e^{i\varphi(P)} \end{aligned} \tag{44}$$

with

$$\tan(\varphi(Q)) = -\frac{Q_2}{Q_1} \tag{45}$$

which can easily be evaluated numerically. In (45) $Q = (Q_0, Q_1, Q_2, Q_3)$ can be either K or P. The spinor-inner-products and thereby the helicity amplitudes can then easily be evaluated numerically by inserting numerical values for the four-momentum components of the momenta as prescribed in (44, 45).

We emphasize that the representation (44) is defined for $Q_0 \geqq 0$ only. If one has to evaluate spinor-inner-products involving momenta with negative energy component, one uses the following rules (see [18]):

$$\begin{aligned} &\langle (-k)p \rangle = \langle k(-p) \rangle = i \langle kp \rangle \\ &\langle (-k)p \rangle^* = \langle k(-p) \rangle^* = i \langle kp \rangle^*. \end{aligned} \tag{46}$$

The rules (46) are motivated by the following observations. The operation $\langle\,\rangle^*$ denotes the complex conjugate of $\langle\,\rangle$ only when the four-momenta involved have a positive energy component. A more general definition of the operation $\langle\,\rangle^*$ is to associate it with

* The breaking of γ^5-invariance in the four-quark case has also been noted in the corresponding e^+e^- four-quark production rate in [16]

* The calculation of traces involving ten and more massless momenta slashed can be considerably simplified by using a new Dirac matrix identity involving massless momenta derived in [17]

the inner product of dotted spinors as in (7).* If one considers (12) with the spinor-inner-products replaced with the contracted forms (6) and (7) it is quite suggestive to associate the momentum spinors with the square roots of momenta. In this sense the factors i in (46) are the square roots of the minus sign of the negative four-momenta in its argument. The rules (46) imply a definite choice of phases for the crossed helicity amplitudes which may differ from the phases that are calculated from the representation of helicity spinors and polarisation vectors in (1, 4, 5). The phase changes implied by (46) have explicitly been compensated for (when necessary) in writing down the crossing relations (27, 28, 41, 42, 43).

3 Squaring the helicity amplitudes

3.1 Colour factors

At the level of helicity amplitudes the colour factors appear only as particular matrix elements of the $SU(3)$ colour matrices. Some care is needed to obtain the correct colour factors when squaring the helicity amplitudes. The colour factors are obtained by taking the relevant colour traces of the contributing products of colour factors. Clearly one does not have a factorization of the colour and the momenta part when squaring the helicity amplitudes. However, it is advantageous and necessary to identify the different colour factors that arise when squaring the helicity amplitudes. This we shall do in the following for the various parton processes. To get the right order of the products of colour matrices one has to carefully keep track of their indices. We discuss the various processes in turn.

i) $q \to qgg$ *or* $\bar{q} \to \bar{q}gg$. The helicity amplitudes have the colour structure (see (24, 25)):

$$h = h^A T^a T^b + h^B T^b T^a. \tag{47}$$

Their moduli squared read

$$|h|^2 = (|h^A|^2 + |h^B|^2) N_C C_F^2 + 2\mathrm{Re}(h^A h^{B*}) N_C C_F (C_F - \tfrac{1}{2} N_C) \tag{48}$$

where $N_C = 3$ is the number of colours and $C_F = \sum_a T^a T^a = (N_C^2 - 1)/(2N_C) = 4/3$. In (48) we have already taken the sum over initial colours. When one squares the helicity amplitudes numerically one first has to identify the coefficients h^A and h^B multiplying $T^a T^b$ and $T^b T^a$, respectively, in (47). Then one has to evaluate $h^A h^{A*}$, $h^A h^{B*}$, ... numerically, and, finally, one multiplies the relevant colour factors as specified in (48).

ii) $g \to gq\bar{q}$. In this case one has one closed fermion line by squaring the diagrams. Therefore these colour factors differ from those of case (i) by an additional trace calculation. Splitting up the helicity amplitudes into "A" and "B" type contributions in the manner of (47) one obtains for the square

$$|h|^2 = (|h^A|^2 + |h^B|^2) T_R C_F (N_C^2 - 1) + 2\mathrm{Re}(h^A h^{B*}) T_R (C_F - \tfrac{1}{2} N_C)(N_C^2 - 1) \tag{49}$$

where $T_R = \mathrm{tr}(T^a T^b) = 1/2$. We have summed over the eight initial state gluon colour indices.

iii) $q \to qq\bar{q}$ *or* $\bar{q} \to \bar{q}q\bar{q}$. The colour accounting is somewhat more complicated in the four-quark case. By squaring the helicity amplitudes diagrammatically one gets different closed fermion lines corresponding to the different bilinears that arise in the product of the sums of terms of the helicity amplitudes. Basically there are two types of colour factors. These are

$$\mathrm{tr}(T^a T^b)\,\mathrm{tr}(T^a T^b) = N_C C_F T_R \tag{50}$$

* [18] took this into consideration by choosing an extra symbol $< >^+$ for the inner product of dotted spinors

Table 2. Four-quark processes in the one-photon approximation. Weight factors for quark and antiquark initiated four-quark processes in the one-photon approximation. Sums and differences of quark parton densities are for hadronic p.c. case as appropriate for the one-photon approximation. The assignment of bilinear terms $(ij) = (ij + ji)$ to the four classes D, D', E and F is as following (refer to Fig. 2 for Feynman diagram labels). (D): 11, 21, 22, 55, 65, 66 (D'): 33, 43, 44, 77, 87, 88 (E): 31, 32, 41, 42, 51, 52, 61, 62, 73, 74, 75, 76, 83, 84, 84, 85, 86 (F): 53, 54, 63, 64, 71, 72, 81, 82

Contr. Feynman diag.'s	$\frac{1}{2s_l+1}$	$\frac{1}{1s_p+1}$	$\frac{1}{N_C}$	Id. part. fact.	Colour factors	Parton densities and charge factors
D	$\frac{1}{2}$	$\frac{1}{2}$	$\frac{1}{3}$	$\frac{1}{2}$	$N_C C_F T_R$	$N_f \sum_{f=1}^{n_f} e_f^2 (q_f + \bar{q}_f)$
D'	$\frac{1}{2}$	$\frac{1}{2}$	$\frac{1}{3}$	$\frac{1}{2}$	$N_C C_F T_R$	$\sum_{f,f'=1}^{n_f,n_{f'}} e_{f'}^2 (q_f + \bar{q}_f)$
E	$\frac{1}{2}$	$\frac{1}{2}$	$\frac{1}{3}$	$\frac{1}{2}$	$N_C C_F (C_F - \frac{1}{2} N_C)$	$\sum_{\substack{f=1 \\ n_f, n_{f'}}}^{n_f} e_f^2 (q_f + \bar{q}_f)$
F	$\frac{1}{2}$	$\frac{1}{2}$	$\frac{1}{3}$	$\frac{1}{2}$	$N_C C_F T_R$	$\sum_{f,f'=1} e_f e_{f'} (q_f - \bar{q}_f)$

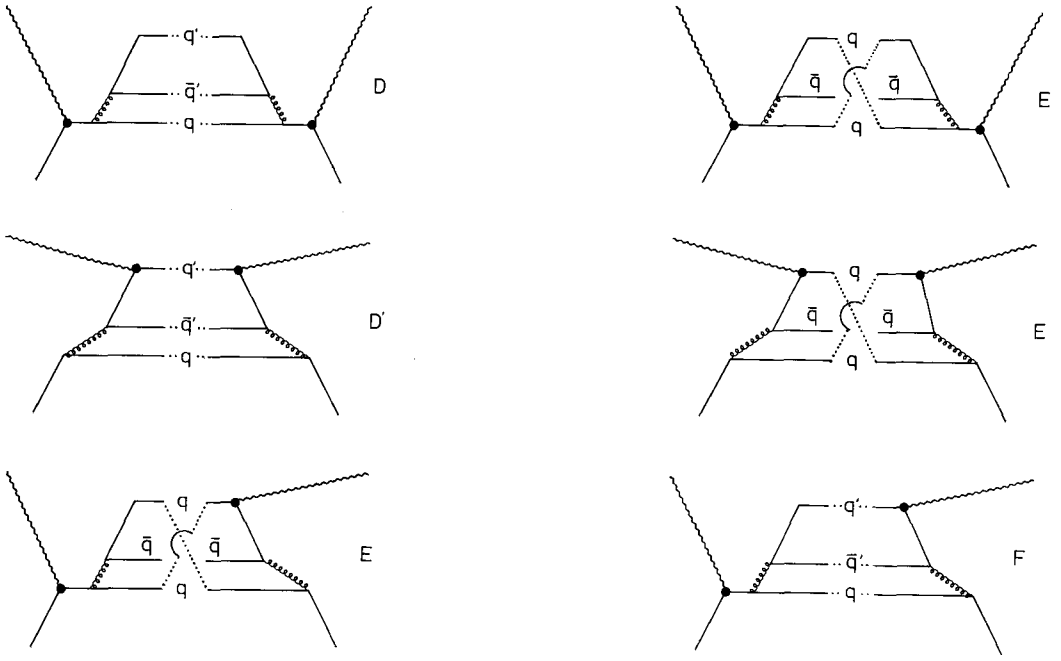

Fig. 3. Generic squared amplitudes contributing to the process (boson $+ q_f \to q_f + q_{f'} + \bar{q}_{f'}$). For the subdivision into classes $D, D' E$ and F see main text

and

$$\mathrm{tr}(T^a T^b T^a T^b) = N_C C_F (C_F - \tfrac{1}{2} N_C) \tag{51}$$

where we have summed over the initial colours.

In order to account for which colour factor multiplies which term in the squared helicity amplitudes one has to refer back to the Feynman diagram decomposition of the helicity amplitudes in (32, 33, 34) and Fig. 2. The correct colour accounting can then be done by following the colour flow in the squared Feynman diagrams. This leads to a classification of the various contributions according to the four classes D, D', E and F. Some representative colour flow diagrams for each of the four classes are drawn in Fig. 3. The resulting colour structure is detailed in Table 2 which also contains a listing of the allocation of various Feynman diagram contributions into the four classes.

3.2 *Squared matrix elements*

We are now in the position to calculate the squared matrix elements of the hard scattering processes. These are obtained by taking the squared moduli of the helicity amplitudes that have been listed in the previous sections. One then does the spin sums by summing over all contributing helicity amplitudes. Finally one sums over all colours.

Before we write down the relevant hard scattering cross-sections we need to specify the neutral current vector and axial vector coupling factors that occur in the standard electroweak model. The coupling of the photon to a quark with flavour f via the vector current is given by the minimal charge coupling $e_f \gamma^\mu$ of the quark (in units of e). The coupling factors of the Z^0 are specified in the following way

hadronic coupling to quark with flavour f:

$$\Gamma^\mu = \frac{v_f}{2\sin 2\theta_W} \gamma^\mu + \frac{a_f}{2\sin 2\theta_W} \gamma^\mu \gamma^5 \tag{52}$$

leptonic coupling:

$$\Gamma^\mu = \frac{v_e}{2\sin 2\theta_W} \gamma^\mu + \frac{a_e}{2\sin 2\theta_W} \gamma^\mu \gamma^5 \tag{53}$$

where

$$\begin{aligned} v_f &= 2t_f - 4e_f \sin^2\theta_W, \quad & a_f &= 2t_f \\ v_e &= -1 + 4\sin^2\theta_W, & a_e &= -1 \end{aligned} \tag{54}$$

t_f denotes the third component of the weak isospin of the f-type quark and e_f represents its charge. θ_W is the Weinberg-angle ($\sin^2\theta_W = 0.217$). The relevant pole propagator factor is $1/(Q^2 + M_Z^2 - iM_Z\Gamma_Z)$ where $Q^2 = -q^2 = -2ll'$. The charged current case (CC) will be treated at the end of Sect. 3.2.

When squaring the amplitudes one will have $\gamma - \gamma, \gamma - Z_0$ and $Z_0 - Z_0$ contributions. When one totals these contributions according to the coupling factors (52, 53) one obtains the Q^2-dependent coupling combinations

$$\begin{aligned} A_f(Q^2) = {} & e_f^2 + 2e_f v_f \Re(\chi_Z)(-v_e + \rho a_e) \\ & + (v_f^2 + a_f^2)|\chi_Z|^2 (v_e^2 + a_e^2 - 2v_e a_e \rho) \end{aligned} \tag{55}$$

$$B_f(Q^2) = 2e_f a_f \Re(\chi_Z)(-a_e + v_e\rho) + 2v_f a_f |\chi_Z|^2(-2v_e a_e - \rho(v_e^2 + a_e^2))$$

where

$$\chi_Z(Q^2) = \frac{1}{(2\sin 2\theta_W)^2} \frac{Q^2}{Q^2 + M_Z^2 - iM_Z\Gamma_Z} \tag{56}$$

and where $\chi_Z(Q^2)$ is the ratio of the Z^0-propagator and the photon propagator times the coupling factor $(2\sin 2\theta_W)^{-2}$.

The coupling combination $A_f(Q^2)$ multiplies the parity-conserving hadronic contributions whereas $B_f(Q^2)$ multiplies the parity-violating hadronic contributions. For later convenience we have included in (55) the necessary additions when one considers polarized lepton deep inelastic scattering, where the longitudinal polarization of the (negatively charged)* lepton is denoted by ρ.

Modifications of the general coupling structure (55) occur for the interference terms in the four-quark case. First, the electroweak currents may couple to different quark flavours in the interference terms, and second, the interference terms show an explicit breaking of γ^5-invariance. We shall return to the complications of the interference term contributions in due course.

In the parton model approach the hard scattering cross-sections are weighted by the parton densities. In order to clearly exhibit the parton that initiates the hard scattering process we write down the hard scattering processes with the parton density weights included. We shall also include the statistical colour and spin factors (from initial state averaging) and the final state identical particle factors in our expressions for the squared matrix elements. The corresponding squared matrix elements will be denoted by a bar. Squared matrix elements corresponding to the unweighted hard scattering process can then be easily obtained by dropping the statistical and the parton density weight factors. In writing down the squared matrix elements for the quark, antiquark and gluon initiated processes we shall take full advantage of the many relations among the helicity amplitudes that have been written down in Sect. 2 in order to simplify the final expressions.

For the various quark, antiquark and gluon initiated processes one then obtains the following expressions:

i) quark and antiquark initiated two quark-two gluon processes $(q_f \to q_f gg) + (\bar{q}_f \to \bar{q}_f gg)$

$$|\overline{M^{4\,\text{jet}}}|^2 = \tfrac{1}{2}\cdot\tfrac{1}{2}\cdot\tfrac{1}{3}\cdot\tfrac{1}{2}\Big\{ A_f(Q^2)\cdot 2 \cdot \sum_{8\,\text{heli}} |h^{vV}_{q_f \to q_f gg}|^2 \otimes (q_f + \bar{q}_f) + B_f(Q^2)\cdot 2 \cdot \sum_{8\,\text{heli}} 2\Re(h^{vV}_{q_f \to q_f gg} h^{aA}_{q_f \to q_f gg}{}^*) \otimes (q_f - \bar{q}_f) \Big\} \tag{57}$$

where q_f and $\bar{q}_f$ denote the quark and antiquark parton densities with flavour f. The numerical factors in the first line of (57) are the initial state averaging factors (lepton spin, parton spin, parton colour) and the final state identical particle factor, in that order. The symbol $\otimes$ stands for the folding in of the parton densities. A similar notation is employed in the following expressions without explicit mention. We have made use of the CP relation (26) to reduce the sum over helicity amplitudes to eight, and have multiplied the resulting expressions by a factor of two.

ii) gluon initiated processes $(g \to g q_f \bar{q}_f)$

$$|\overline{M^{4\,\text{jet}}}|^2 = \tfrac{1}{2}\cdot\tfrac{1}{2}\cdot\tfrac{1}{8}\cdot\tfrac{1}{2}\Big\{ A_{f'}(Q^2)\cdot 2 \cdot \sum_{8\,\text{heli}} |h^{vV}_{g \to g q_{f'} \bar{q}_{f'}}|^2 \otimes g + B_{f'}(Q^2)\cdot 2 \cdot \sum_{8\,\text{heli}} 2\Re(h^{vV}_{g \to g q_{f'} \bar{q}_{f'}} h^{aA}_{g \to g q_{f'} \bar{q}_{f'}}{}^*) \otimes g \Big\} \tag{58}$$

g is the gluon parton density. Again we have made use of the CP relation (26) to reduce the sum over helicity amplitudes to eight and multiplied the result by an overall factor of two. Note that the parity violating VA contribution in (58) proportional to $B_f(Q^2)$ is antisymmetric under $q \leftrightarrow \bar{q}$ exchange due to charge conjugation invariance. Its detection would require flavour tagging of the produced quarks and antiquarks.

iii) quark and antiquark initiated four-quark process $(q_f \to q_f q_{f'} \bar{q}_{f'}) + (\bar{q}_f \to \bar{q}_f q_{f'} \bar{q}_{f'})$. We shall first list the none-interference contributions from the classes D, D' and E. The structure of the interference contributions F is more involved and requires separate discussion. For the $D + D' + E$ contributions one has

$$\begin{aligned} |\overline{M^{4\,\text{jet}}}|^2_{D+D'+E} = \tfrac{1}{2}\cdot\tfrac{1}{2}\cdot\tfrac{1}{3}\cdot\tfrac{1}{2}\Big\{ & A_f(Q^2)\cdot 2 \cdot \sum_{6\,\text{heli}} \sum_{D,E} |h^{vV}_{q_f \to q_f q_f \bar{q}_f}|^2 \otimes (q_f + \bar{q}_f) \\ & + B_f(Q^2)\cdot 2 \cdot \sum_{6\,\text{heli}} \sum_{D,E} 2\Re(h^{vV}_{q_f \to q_f q_f \bar{q}_f} \cdot h^{aA}_{q_f \to q_f q_f \bar{q}_f}{}^*) \otimes (q_f - \bar{q}_f) \\ & + A_{f'}(Q^2)\cdot 2 \cdot \sum_{6\,\text{heli}} \sum_{D'} |h^{vV}_{q_f \to q_f q_{f'} \bar{q}_{f'}}|^2 \otimes (q_f + \bar{q}_f) \\ & + B_{f'}(Q^2)\cdot 2 \cdot \sum_{6\,\text{heli}} \sum_{D'} 2\Re(h^{vV}_{q_f \to q_f q_{f'} \bar{q}_{f'}} \cdot h^{aA}_{q_f \to q_f q_{f'} \bar{q}_{f'}}{}^*) \otimes (q_f - \bar{q}_f). \end{aligned} \tag{59}$$

We have decided to drop the distinction between

* The description of DIS with positively charged leptons leads to minor modifications in (55) which are detailed in [5]

the equal and the unequal flavour cases and have summed over 2 times 6 helicity amplitudes in both cases. The overcounting in the unequal flavour case ($f \neq f'$) is compensated by our multiplication of these contribution with the Fermi statistical factor $\frac{1}{2}$ as in the equal flavour case ($f = f'$). As in the above two quark-two gluon cases the sum over helicities runs over one-half of the contributing helicity amplitudes due to the use of CP relations with a factor of two included to obtain the correct final answer.

As mentioned in Sect. 3 there are two different colour factors depending on which bilinear combination of Feynman diagrams one is considering. As discussed in Sect. 3.1 we have accordingly divided the various bilinear contributions *within one* squared helicity amplitude into the classes D, D', E and F with the appropriate colour factors given in Table 2*. Table 2 also contains the colour and spin factors (from initial state averaging) and the final state identical particle statistics factor. The last column in Table 2 contains the appropriate charge coupling factors for the pure one-photon exchange case. Note that we have summed over all quark flavours in the last column of Table 2.

The generalisation of the last column in Table 2 to the general standard model electroweak case is then obvious. For the classes D, D' and E one replaces e_f^2 ($e_{f'}^2$) by the coupling combinations $A_f(Q^2)(A_{f'}(Q^2))$ and $B_f(Q^2)(B_{f'}(Q^2))$ of (55) for the pc and pv hadronic contributions, respectively, as already stated in (57–59).

The interference contributions class F involve the calculation of two separate fermion traces (see Fig. 3). It is then immediately obvious that these contributions show explicit breaking of γ^5-invariance, i.e. one finds $AA \neq VV$ and $AV \neq VA$ for the hadronic contributions**. Thus one cannot expect as simple a coupling structure as is true for the two quark-two gluon and the diagonal four-quark contributions. Also the neutral electroweak current may couple to different flavours $f \neq f'$ in the interference terms. In addition, the association of the parton density combinations $(q + \bar{q})$ and $(q - \bar{q})$ with pc and pv hadronic contributions is no longer true for the interference contributions. They involve a product of traces of 3 fermion (or antifermion) propagators and the associated γ^μ or $\gamma^\mu\gamma^5$ couplings. Each such trace is antisymmetric (symmetric) under quark-antiquark exchange for the vector current (axial vector current) due to charge conjugation invariance. Thus one has both symmetric and antisymmetric terms under $q \leftrightarrow \bar{q}$ exchange for *both* the produced $q \leftrightarrow \bar{q}$ pair of the final state and for $q \leftrightarrow \bar{q}$ exchange of the initial state quark against an antiquark. Taking all these considerations into account we finally arrive at the following interference structure resulting from the class F contributions:

$$
\begin{aligned}
|\overline{M^{4\,\text{jet}}}|_F^2 = \tfrac{1}{2}\cdot\tfrac{1}{2}\cdot\tfrac{1}{3}\cdot\tfrac{1}{2}\Big\{ & A'_{ff'}(Q^2)\cdot 2 \\
& \cdot \sum_{6\,\text{heli}} \sum_{F} |h^{vV}_{q_f \to q_f q_{f'} \bar{q}_{f'}}|^2 \otimes (q_f - \bar{q}_f) \\
& + A''_{ff'}(Q^2)\cdot 2 \cdot \sum_{6\,\text{heli}} \sum_{F} |h^{vA}_{q_f \to q_f q_{f'} \bar{q}_{f'}}|^2 \\
& \cdot \otimes (q_f + \bar{q}_f) + B'_{ff'}(Q^2)\cdot 2 \\
& \cdot \sum_{6\,\text{heli}} \sum_{F'} 2\Re(h^{vV}_{q_f \to q_f q_{f'} \bar{q}_{f'}}(i) h^{aA}_{q_f \to q_f q_{f'} \bar{q}_{f'}}(j)^*) \\
& \cdot \otimes (q_f + \bar{q}_f) + B''_{ff'}(Q^2)\cdot 2 \\
& \cdot \sum_{6\,\text{heli}} \sum_{F'} 2\Re(h^{vA}_{q_f \to q_f q_{f'} \bar{q}_{f'}}(i) h^{aV}_{q_f \to q_f q_{f'} \bar{q}_{f'}}(j)^*) \\
& \cdot \otimes (q_f - \bar{q}_f) \Big\}. \qquad (60)
\end{aligned}
$$

For the VA interference terms in (60) one has to take into account the ordered subset F' of bilinear Feynman diagram contributions where

$$F' := \{(35),(45),(36),(46),(71),(72),(81),(82)\} \quad \text{ordered.}$$

The flavour coupling coefficients appearing in (60) are given by*

$$
\begin{aligned}
A'_{ff'}(Q^2) &= e_f e_{f'} + (e_f v_{f'} + e_{f'} v_f)\Re(\chi_Z)(-v_e + \rho a_e) \\
&\quad + v_f v_{f'} |\chi_Z|^2 (v_e^2 + a_e^2 - 2 v_e a_e \rho) \\
A''_{ff'}(Q^2) &= a_f a_{f'} |\chi_Z|^2 (v_e^2 + a_e^2 - 2 v_e a_e \rho) \\
B'_{ff'}(Q^2) &= e_f a_{f'} \Re(\chi_Z)(-a_e + \rho v_e) + v_f a_{f'} |\chi_Z|^2 \\
&\quad \cdot (-2 v_e a_e - \rho(v_e^2 + a_e^2)) \\
B''_{ff'}(Q^2) &= e_{f'} a_f \Re(\chi_Z)(-a_e + \rho v_e) + v_{f'} a_f |\chi_Z|^2 \\
&\quad \cdot (-2 v_e a_e - \rho(v_e^2 + a_e^2)). \qquad (61)
\end{aligned}
$$

One notes that the electroweak coupling structure (61) is somewhat more complicated for the interference contributions F than for the non-interference contributions D, D' and E due to the breaking of γ^5-invariance.

It is quite clear that one is not sensitive to the interference term contributions in the VV coupling case if one does not identify the flavour of the produced quarks and antiquarks. Thus class F does not contribute to the *total* cross-section in the one-photon exchange approximation. This is no longer true in

* Representative contributions of each class have been drawn in Fig. 3, where the colour and charge coupling factors can be read off from the colour and charge flow of the various diagrams

** This is most easily seen by using Fierz identities to rewrite the products of two traces into one trace. Then the breaking of γ^5-invariance becomes quite manifest

* Note that we do not obtain an overall pv contribution to the cross-section from the interference term (i.e. odd in the total number of pv couplings) as we are neglecting the imaginary part of the 2-propagator in the class F interference terms (see also [16])

general for the VA, AV and AA coupling cases since the axial vector coupling may occur in the *produced fermion* loop leading to a symmetric distribution in the quark and antiquark momenta with the consequence that one has class F contributions to the total cross-section without flavour identification.

We close this section by listing the changes necessary to obtain the deep inelastic charged current scattering case. The squared matrix elements for the charged current case for the quark (antiquark) initiated two quark-two gluon case can be obtained from (57) by the replacement

$$\begin{aligned} A_f(Q^2) &\to \tfrac{1}{2}(1-\rho)|\chi_W|^2|V_{ff'}|^2 \\ B_f(Q^2) &\to -\tfrac{1}{2}(1-\rho)|\chi_W|^2|V_{ff'}|^2 \end{aligned} \tag{62}$$

where

$$\chi_W = \frac{1}{(2\sin\theta_W)}\frac{Q^2}{Q^2+M_W^2-iM_W\Gamma_W} \tag{63}$$

and where $V_{ff'}$ is the Kobayashi–Maskawa matrix element for the charged current $f \to f'$ transitions.

It is clear that the number of helicity amplitudes to be summed in the charged current case is reduced by a factor of two since the neutrino (antineutrino) is in a definite helicity state.

Corresponding changes have to be done in the gluon-initiated process (58) and the four-quark process (59). Note that there are no class F interference contributions in the four-quark charged current processes because of charge conservation (see Fig. 3).

4 Differential cross section

We now proceed with the study of the differential cross-section for electron (positron) proton scattering

$$e^{\pm}(l) + \mathscr{P}(P) \to e^{\pm}(l') + 4\,\text{jets}. \tag{64}$$

In the QCD improved quark parton model, the cross-section for the hadronic process (64) can be written as an incoherent sum of the contributions of each parton type (quarks, antiquarks and gluons) within the proton. Each of the parton carries a fraction η of the proton total momentum. The hadronic cross-section is obtained by folding the partonic cross-section with the parton densities within the proton. One thus obtains

$$\sigma_H(P) = \sum_{i=-n_f}^{n_f} \int_0^1 d\eta f_i(\eta, \mu_F^2)\hat{\sigma}_i(\eta P, \mu_R^2) \tag{65}$$

where the index i refers to the nature of the incoming parton (gluon: $i=0$, n_f light quarks: $i=1,\ldots,n_f$, and n_f light antiquarks: $i=-n_f\cdots-1$). $\hat{\sigma}_i$ is the partonic cross-section initiated by the parton i with momentum p and $f_i(\eta,\mu_F^2)$ is the probability of finding this parton in the proton with the momentum fraction η (i.e. $p=\eta P$). We have also indicated the scale dependence of the cross-section. It depends on two mass scales: μ_F is the factorization mass in the parton densities and μ_R the renormalization mass entering the strong coupling constant.

The $O(\alpha_s^2)$ $2\to4$ differential parton cross-section $d\hat{\sigma}_P$ may be written as

$$d\hat{\sigma}_i = \frac{1}{2s_p}|\overline{M_i^{4\,\text{jet}}}|^2 dPS^{(4)}. \tag{66}$$

Here $|\overline{M_i^{4\,\text{jet}}}|^2$ is the squared matrix element of the parton process initiated by parton i including all coupling, statistical, colour and propagator factors as given in Sect. 3.2 (see (57–60)).

The Lorentz invariant four-particle phase space is given by:

$$\begin{aligned} dPS^{(4)} = (2\pi)^4\delta^4(l+p-l'-p_1-p_2-p_3) \\ \cdot\frac{d^3l'}{(2\pi)^3 2E'}\frac{d^3p_1}{(2\pi)^3 2E_1}\frac{d^3p_2}{(2\pi)^3 2E_2}\frac{d^3p_3}{(2\pi)^3 2E_3} \end{aligned} \tag{67}$$

where the momenta are defined in Fig. 1. The squared partonic cms energy s_p is related to the total squared cms energy, s, via

$$s_p \equiv (p+l)^2 = \eta s \equiv \eta(P+l)^2. \tag{68}$$

Besides a trivial azimuthal integration the subprocess (66) is determined by seven kinematical variables which we choose as $y, Q^2, z, \Phi, s_{23}, \cos\theta_{23}$ and Φ_{23}. Here y and Q^2 are the standard DIS variables defined by:

$$\begin{aligned} y &= \frac{Pq}{Pl} \quad Q^2 = -(l-l')^2 = xys \\ W^2 &= (P+q)^2 = (1-x)ys. \end{aligned} \tag{69}$$

The squared invariant mass of partons 2 and 3 is denoted by s_{23}:

$$s_{23} = (p_2+p_3)^2. \tag{70}$$

In terms of invariants the variable z is given by

$$z = 1 - \frac{pp_1}{pq}. \tag{71}$$

In the (boson-initial parton) cms, $\mathbf{p}+\mathbf{q}=0$, (with the incoming parton defining the positive z-axis) z is related to the angle θ between the momentum $\mathbf{p}_1$ of parton 1 and the momentum $\mathbf{p}$ of the incoming parton via:

$$\cos\theta = \frac{(2z-1)\hat{s} - s_{23}}{\hat{s} - s_{23}}. \tag{72}$$

Here $\hat{s}$ is the squared invariant mass of the (boson-initial parton) subsystem:

$$\hat{s} = (p+q)^2 = y\eta s - Q^2 \tag{73}$$

Φ is the azimuthal angle of the outgoing lepton in the (boson-initial parton) cms. Finally, θ_{23} and Φ_{23} are the polar and aximuthal angles of parton 2 in the rest frame $\mathbf{p}_2+\mathbf{p}_3=0$. In terms of these variables the phase

space can be decomposed as:*

$$\int_0^1 d\eta \int dPS^{(4)}(s_p) = \frac{1}{2^{14}\pi^7} \int_0^1 dy \int_0^{ys} dQ^2 \int_x^1 d\eta \int_0^1 dz \int_0^{2\pi} d\Phi \int_0^{z\hat{s}} ds_{23} \cdot \int_{-1}^{+1} d\cos\theta_{23} \int_0^{2\pi} d\Phi_{23}. \quad (74)$$

Now the cross-section of leptoproduction in $O(\alpha_s^2)$ can be written as:

$$\frac{(2\pi)^2 d^8\sigma_H}{dy dQ^2 d\eta dz d\Phi ds_{23} d\cos\theta_{23} d\Phi_{23}} = \sum_{i=-n_f}^{n_f} \left(\frac{\alpha_s(\mu_R^2)}{2\pi}\right)^2 \frac{\pi\alpha^2}{8\eta s} f_i(\eta, \mu_F^2) |\overline{M_i^{4\,\text{jet}}}|^2. \quad (75)$$

We close this section by remarking that one can save on numerical integration time by doing the Φ integration in (75) analytically. The explicit representation of the incoming lepton momentum in the (boson-initial parton) cms is given by:

$$l = E_l(1, \sin\beta\cos\Phi, -\sin\beta\sin\Phi, \cos\beta) \quad (76)$$

where

$$E_l = \frac{\hat{s} + (1-y)Q^2}{2\sqrt{\hat{s}}} \quad \cos\beta = \frac{(1-y)Q^2 - \hat{s}}{(1-y)Q^2 + \hat{s}}. \quad (77)$$

The most general Φ-dependent integrands involve up to two contractions with the lepton momenta. It is then easy to show that:

$$\int_0^{2\pi} d\Phi \frac{pp'}{2\pi} = pp'$$

$$\int_0^{2\pi} d\Phi \frac{lp}{2\pi} = \tilde{l}'p$$

$$\int_0^{2\pi} d\Phi \frac{(lp)(lp')}{2\pi} = (\tilde{l}p)(\tilde{l}'p) + \frac{(1-y)Q^2}{2y^2}(p_x p'_x + p_y p'_y) \quad (78)$$

where $\tilde{l} = E_l(1, 0, 0, \cos\beta)$ and p and p' are any two momenta not depending on Φ. Corresponding integrands involving l' can be written in the form (78) by using $q = l - l'$.

5 Numerical results

We shall now turn to our numerical cross-section results. We have decided to limit our discussion to the case of unpolarized electron-proton scattering in the one-photon exchange approximation which is the dominant contribution at HERA energies. To be sure on our numerical results we have numerically checked the helicity method one-photon exchange parton cross sections derived in this paper against the corresponding covariant expressions obtained from [20] and [21]* through crossing. We hope to return to an investigation of the $\gamma - Z^0$, $Z^0 - Z^0$ and charged current jet production rates at a later time.

We use the parton density parametrization set 1 of [22] and the one-loop formula of the strong coupling constant

$$\alpha_s(\mu_R^2) = \frac{12\pi}{(33 - 2N_f)\ln(\mu_R^2/\Lambda^2)}. \quad (79)$$

In order to be consistent with the Q^2 evolution of the parton densities the values for the QCD scale parameter, Λ, and for the number of flavours, N_f, in (79) are taken as in the parametrization of [22], i.e. $\Lambda = 0.2\,\text{GeV}$ and $N_f = 6$. We restrict the number of (massless) quark flavours in the proton that can initiate the higher order parton processes to $n_f = 4$. Similarly we include $n_f = 4$ (massless) quark flavours that can be pair-produced. There is some freedom in the choice of the mass scales μ_R and μ_F. In DIS scattering it is natural to take $\mu_R^2 = \mu_F^2 = Q^2$. The electroweak coupling constant α is assumed to be constant over the range of energies considered in this paper, i.e. $\alpha = 1/137$.

Finally we have to define the deep inelastic scattering region. We choose the lower bounds:

$$Q^2 \geqq Q_0^2 \equiv 4\,\text{GeV}^2 \quad W^2 \geqq W_0^2 \equiv 5\,\text{GeV}^2$$
$$x \geqq x_0 \equiv 10^{-3}. \quad (80)$$

The lower limits in Q^2 and x are prescribed by the parametrization of the parton densities. $Q^2 = 4\,\text{GeV}^2$ is the mass value from which the parton densities are evolved. Below $x < 10^{-3}$ the parton density parametrization is uncertain. One also has to limit W^2 from below in order to insure an appropriate hadronic final state. When producing well separated multijet final states the effective lower limit on W^2 will actually be increased (see below).

When calculating the $O(\alpha_s^2)$ tree graph cross-sections in the above region one encounters infrared/mass (IR/M) singularities. They originate from the emission of soft and/or collinear partons. It is clear that the tree graph cross-sections make sense only for the production of well separated hard jets. One possibility to exclude the singular regions of phase space is the introduction of energy and angle cuts. However, as elaborated in [5] and [23], energy-angle cuts are not suitable for an asymmetric machine with its strong boost from the hadronic cms to the laboratory frame. Instead we prevent the internal virtual particles to reach their mass shell by imposing an invariant mass cut

$$s_{ij} > s_0 \quad s_{ij} \equiv (p_i + p_j)^2, \quad i \neq j = 1, 2, 3, 4. \quad (81)$$

* A quick check of the phase space decomposition (74) is afforded by an explicit integration of the r.h.s with an integrand 1 which gives $(2\pi)^{-5} 3^{-2} s^2$. This result can be checked against the general formula given e.g. in [19] who obtain the general n-particle result $PS^{(n)}(s_p) = (2\pi)^{4-3n}(\pi/2)^{n-1} s_p^{n-2}/((n-1)!(n-2)!)$ which agrees with the latter result for $n = 4$ which integrated over η from 0 to 1 ($s_p = \eta s$)

* Note that the four-quark annihilation rate written down in [21] is too small by a factor of 2

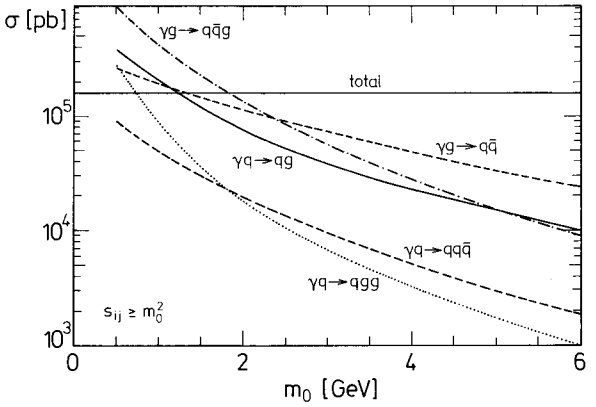

Fig. 4. Invariant mass cut-off dependence of the various $O(\alpha_s^2)$ and $O(\alpha_s)$ processes. The cut-off m_0 is defined by $s_{ij} \geqq m_0^2$. Also shown is the total cross-section

The finite tree graph cross-sections were then evaluated using the Monte Carlo integration routines VEGAS [24] and DIVON4 [25]. We achieved a major improvement on our integration efficiency by explicitly incorporating the constraints (80, 81) into the phase space boundaries (see (74)).

One possible choice for s_0 is a fixed cut, $s_0 = m_0^2$. Although a fixed mass cut will not be our final preferred choice it provides for a first cursory exposition of the order of magnitude size of the 4-jet cross sections. This procedure would be reminiscent of the e^+e^- case where one demands the invariant masses, s_{ij}, to be larger than a given constant value for a given fixed value of the squared cms energy Q^2. Note that the choice $s_0 = m_0^2$ in (81) may increase the lower limit in the hadronic mass W^2 according to

$$\begin{aligned} W^2_{\min} &= \max(W_0^2, 3m_0^2) \quad \text{in} \quad O(\alpha_s) \\ W^2_{\min} &= \max(W_0^2, 6m_0^2) \quad \text{in} \quad O(\alpha_s^2) \end{aligned} \tag{82}$$

since in $O(\alpha_s)$ $W^2 = (p_1 + p_2 + p_3)^2 = s_{12} + s_{13} + s_{23} \geqq 3s_0$ and in $O(\alpha_s^2)$ $W^2 = \left(\sum_{i=1}^{4} p_i\right)^2 = s_{12} + \cdots + s_{34} \geqq 6s_0$.

In Fig. 4 we show the dependence of the 4-jet cross-sections on the cut value m_0. Also shown is the m_0-dependence of the $O(\alpha_s)$ tree graph cross-sections and the (m_0-independent) total DIS cross-section. The $O(\alpha_s)$ processes, $\gamma^* q \to qg$ and $\gamma^* g \to q\bar{q}$, are also subject to the resolution criterium (81). The total DIS cross-section drawn in Fig. 4 is approximated by the quark parton model result (see e.g. (6) in [5]). We find that the 4-jet cross-sections show a steep increase as the constant cut m_0 becomes smaller. The steepest increase occurs for the quark initiated process $\gamma^* q \to qgg$ whereas the small m_0-behaviour is somewhat milder for $\gamma^* q \to qq\bar{q}$ and $\gamma^* g \to gq\bar{q}$. The $O(\alpha_s)$ cross-sections show a slower increase with decreasing m_0 where the gluon-initiated process is least sensitive.

Whereas the quark initiated processes in $O(\alpha_s)$ and in $O(\alpha_s^2)$ dominate for small m_0, the gluon initiated processes are larger at large values of m_0. The dominance of the latter at large m_0 originates from the corresponding ratio of the parton densities whereas the small m_0-behaviour of the 4-jet and the 3-jet cross-sections can be understood from the singular behaviour of the respective partonic cross-sections in the small m_0 limit. The lower limit on η, the momentum fraction of the incoming parton, can be derived from the following relations:

i) in $O(\alpha_s)$: $\hat{s} = (p_1 + p_2)^2 = s_{12} \geqq s_0$
ii) in $O(\alpha_s^2)$: $\hat{s} = (p_1 + p_2 + p_3)^2 = s_{12} + s_{13} + s_{23} \geqq 3s_0$.

We find:

$$\begin{aligned} \eta_{\min} &= x + \frac{m_0^2}{ys} \\ \eta_{\min} &= x + \frac{3m_0^2}{ys}. \end{aligned} \tag{83}$$

Thus even for m_0 as large as $m_0 = 6\,\text{GeV}$ we have $\eta_{\min} = 2 \times 10^{-3}$. Now at these small values of η the gluon density is much larger than the quark densities which explains why the gluon-initiated cross-sections are so large. As m_0 becomes smaller the lower limit on η changes only slightly to 10^{-3}. Thus it is not the parton densities that determine the small m_0-behaviour, but the small m_0-behaviour of the partonic cross-sections.

For the 3-jet case the leading singular behaviour is given by $\gamma^* q \to qg \propto \ln^2 m_0$ and $\gamma^* g \to q\bar{q} \propto \ln m_0$ as $m_0 \to 0$. This is quite evident in the small m_0-behaviour of the corresponding 3-jet rates shown in Fig. 4. The corresponding 4-jet cases can then be read off from the known singular behaviour of the Atarelli–Parisi splitting functions according to the following diagrammatic representation:

$$(\gamma^* q \to qg)_{\ln^2 m_0} \begin{array}{l} \xrightarrow{q \to qg} (\gamma^* q \to qgg) \propto \ln^4 m_0 \\ \xrightarrow{g \to q\bar{q}} (\gamma^* q \to qq\bar{q}) \propto \ln^3 m_0 \end{array} \tag{84}$$

and

$$(\gamma^* g \to q\bar{q})_{\ln m_0} \xrightarrow{q \to qg} (\gamma^* g \to gq\bar{q}) \propto \ln^3 m_0. \tag{85}$$

This singularity structure can in fact be observed in Fig. 4 as m_0 becomes small.

An inspection of Fig. 4 shows that $\sigma(4\text{-jet}) \geqq \sigma(3\text{-jet})$ when $m_0 \leqq 5.5\,\text{GeV}$. From the perturbative point of view this is not acceptable as the $O(\alpha_s^2)$ jet rates would exceed the $O(\alpha_s)$ jet rates. With such a small cut one is probing the singular regions and not the perturbative jet regime. In order for perturbation theory to make sense one has to choose $m_0 \geqq 5.5\,\text{GeV}$ in order to insure that $\sigma(4\text{-jet}) \leqq \sigma(3\text{-jet})$. But even then a closer look at the jet rates in different regions of phase space reveals that there are regions in x and Q^2 where the $O(\alpha_s^2)$ 4-jet rate still exceeds the $O(\alpha_s)$ 3-jet rate even if the total rate does not. A similar behaviour had been observed to be true for the corresponding 3-jet/2-jet

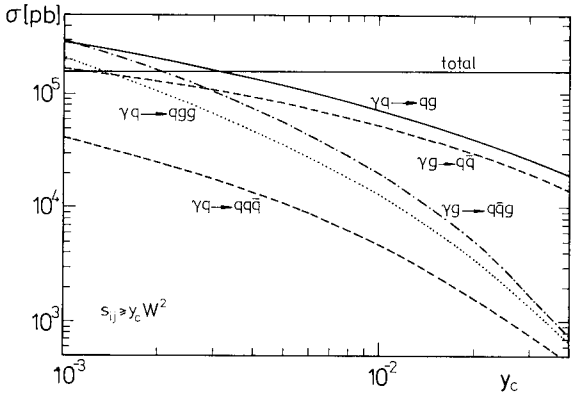

Fig. 5. Invariant mass cut-off dependence of the various $O(\alpha_s^2)$ and $O(\alpha_s)$ processes. The cut-off y_c is defined by $s_{ij} \geqq y_c W^2$

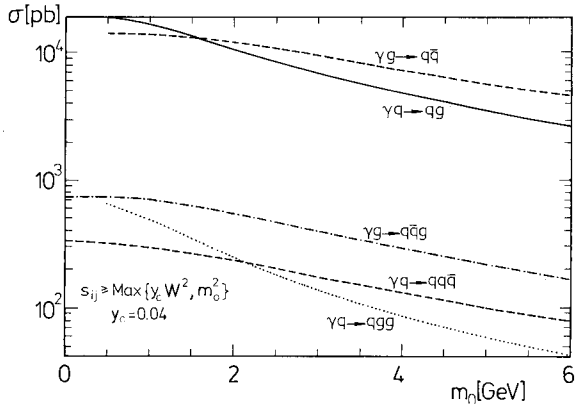

Fig. 6. Invariant mass cut-off dependence of the various $O(\alpha_s^2)$ and $O(\alpha_s)$ processes. The cut-off m_0 is defined by $s_{ij} \geqq \max(m_0^2, y_c W^2)$, (89), with $y_c = 0.04$

ratios in [5]. As in [5] we are forced to the conclusion that a fixed invariant mass cut is not an acceptable physical choice for jet definition.

A better cut-off choice can be found by investigating the origin of the logarithmic terms in (84, 85). As an example consider the z integration of the $O(\alpha_s)$ process $\gamma^* + q \to q + g$. The leading term is

$$\int_{z_0}^{1-z_0} \frac{dz}{1-z} = \ln\left(\frac{z_0}{1-z_0}\right) \qquad z_0 = \frac{s_0}{(1-\eta)ys}. \tag{86}$$

Clearly, for fixed $s_0 = m_0^2$ these logarithmic terms strongly vary with η, y and z or equivalently with $p_\perp$ or the rapidity of the jets. If one replaces m_0 by an invariant mass cut that scales with an internal mass M, one will temper this dependence and thus prevent an unphysical growth of the total and differential cross-sections. These observations lead us to the cut-off choice:

$$s_{ij} \geqq y_c M^2. \tag{87}$$

The problem in deep inelastic scattering is the non-uniqueness of the choice of mass scale M, which could be W, Q or $\sqrt{\hat{s}}$ or linear combinations of them. In the case of 3-jet production investigated in [5] we found the invariant $W^2 = (1-x)ys$ to be a preferred choice of mass scale from the physics point of view. We shall subsequently also use W^2 as mass scale in the invariant mass cut (87) in the 4-jet production case.

In Fig. 5 we plot the 3- and 4-jet cross-sections as a function of y_c. We indeed observe an improvement compared to Fig. 4. The ratios of the various processes are now approximately constant when varying the cut y_c. The hierarchy of the various parton processes is partly due to the behaviour of parton densities and partly due to the limiting behaviour of the partonic cross-sections. The condition (87) with $M \equiv W$ does not change the lower limit on W^2 but modifies the available η range:

$$W^2 \geqq W_0^2 \tag{88}$$

$$\eta \geqq 3y_c + x(1-3y_c) \quad \text{in} \quad O(\alpha_s^2)$$

$$\eta \geqq y_c + x(1-y_c) \quad \text{in} \quad O(\alpha_s)$$

Hence the parton densities, $f_i(\eta, Q^2)$, are only probed at modest values of η for y_c not too small. We do observe, however, that the cross-sections steeply increase as y_c decreases. Moreover, the 4-jet rates exceed the 3-jet rates when y_c falls below $\approx 3 \cdot 10^{-3}$. W^2 is limited from below by W_0^2, (88). Thus for small y_c values the absolute lower limit on the invariant masses is exceedingly tiny. For example, with $y_c = 0.002$ we obtain $s_{ij} \geqq 0.01\ \mathrm{GeV}^2$. This leads to too small invariant masses for a perturbative calculation to be meaningful. We therefore impose an additional fixed mass cut m_0 in order to clearly separate the perturbative and nonperturbative regime. The invariant mass cut now becomes:

$$s_{ij} \geqq \max\{y_c W^2, m_0^2\}. \tag{89}$$

In Fig. 6 we plot jet rates as a function of m_0 with y_c held fixed at $y_c = 0.04$. The dependence of the various cross-sections on m_0 is much weaker now, (compare with Fig. 4). Also the 4-jet/3-jet ratios are rather stable and take the values of approximately α_s/π. For small $m_0 \leqq 2\ \mathrm{GeV}$ one observes a cross-over of $\gamma^* q \to qgg$ as compared to $\gamma^* g \to gq\bar{q}$ and $\gamma^* q \to qq\bar{q}$ on the one hand and $\gamma^* q \to qg$ compared to $\gamma^* g \to q\bar{q}$ on the other hand. This can again be traced to the small m_0 singularity structure of the various cross-sections as given in (84, 85). We believe that a reasonable choice for the fixed mass cut in (89) is $m_0 = 2\ \mathrm{GeV}$. Such a choice would be in agreement with the experience gained in the 3- and 4-jet analysis in e^+e^--interactions. For y_c we choose $y_c = 0.04$ following again the lessons learned in e^+e^--interactions. Our subsequent analysis is then based on the invariant mass cut

$$s_{ij} \geqq \max\{0.04W^2, 4\mathrm{GeV}^2\}. \tag{90}$$

We would like to emphasize that the invariant mass

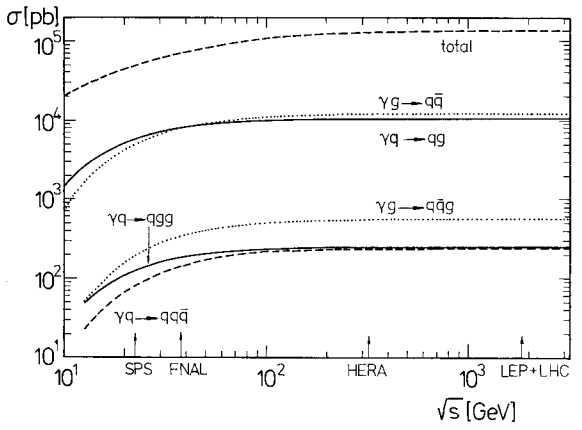

Fig. 7. Dependence of the total cross-section and the various $O(\alpha_s^2)$ and $O(\alpha_s)$ processes on the total cms energy $\sqrt{s}$. The cut-off values in (89) are $y_c = 0.04$ and $m_0 = 2\,\text{GeV}$

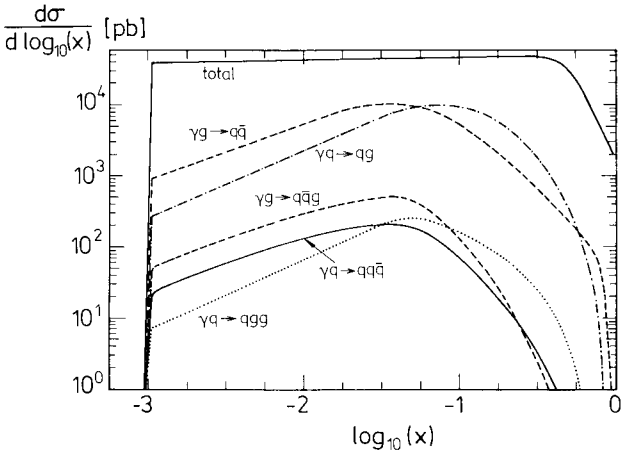

Fig. 8. x-dependence of the total cross-section and the various $O(\alpha_s^2)$ and $O(\alpha_s)$ processes. The cut-off values in (89) are $y_c = 0.04$ and $m_0 = 2\,\text{GeV}$

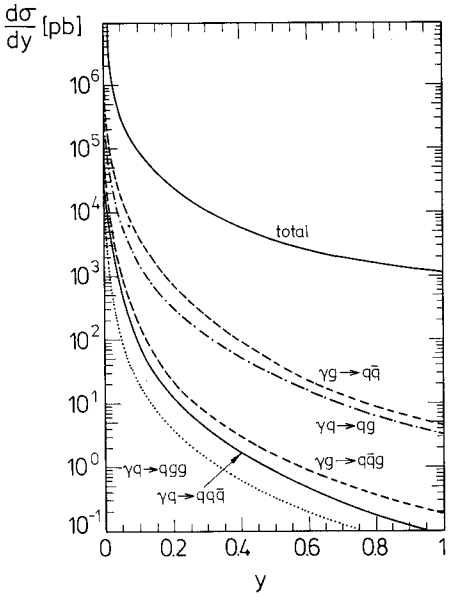

Fig. 9, y-dependence of the total cross-section and the various $O(\alpha_s^2)$ and $O(\alpha_s)$ processes. The cut-off values in (89) are $y_c = 0.04$ and $m_0 = 2\,\text{GeV}$

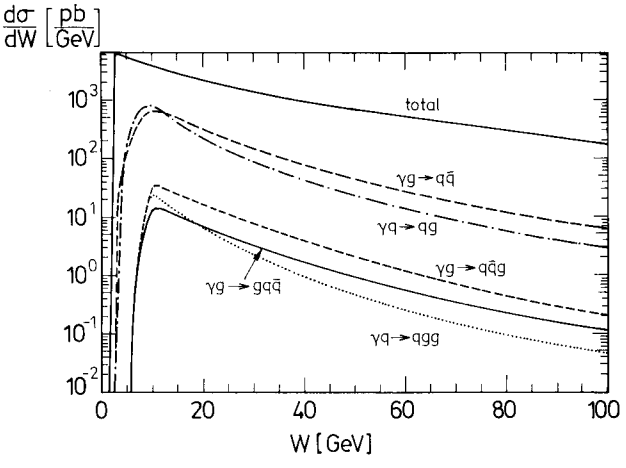

Fig. 10. W-dependence of the total cross-section and the various $O(\alpha_s^2)$ and $O(\alpha_s)$ processes. The cut-off values in (89) are $y_c = 0.04$ and $m_0 = 2\,\text{GeV}$

cut (90) introduces a characteristic difference between the available ranges in η and W^2 for the $O(\alpha_s)$ 3-jet and $O(\alpha_s^2)$ 4-jet cases. We have:

$$
\begin{aligned}
&W^2 \geqq \max(W_0^2, 6m_0^2) = 24\,\text{GeV}^2;\\
&\eta \geqq 3y_c + x(1-3y_c) = 0.12 \quad \text{in} \quad O(\alpha_s^2)\\
&W^2 \geqq \max(W_0^2, 3m_0^2) = 12\,\text{GeV}^2;\\
&\eta \geqq y_c + x(1-y_c) = 0.04 \qquad \text{in} \quad O(\alpha_s).
\end{aligned}
\tag{91}
$$

The pattern of (91) can be seen to generalize to higher jet multiplicities: the higher the jet multiplicity the higher the required amount of hadronic energy W. This can only be achieved by a more energetic incoming parton, i.e. the lower bound on η has to increase with the jet multiplicity. This means that multijet final states see less of the sea contributions within the proton, in particular the gluon initiated processes will become less important.

In Fig. 7 we show how the various cross-sections vary with a given invariant energy $\sqrt{s}$. The range of energies spans the CERN SPS ($\sqrt{s} \approx 2\,\text{GeV}$) to the LEP and LHC option ($\sqrt{s} \approx 2 \cdot 10^3\,\text{GeV}$). One observes an increase with $\sqrt{s}$ of all cross-sections where the increase is somewhat steeper for lower energies. In the 3-jet case there is a cross-over at FNAL-energies ($\sqrt{s} \approx 4\,\text{GeV}$). In the 4-jet case the process $\gamma^* g \to q\bar{q}$ dominates over the whole $\sqrt{s}$ range, whereas $\gamma^* q \to qgg$ and $\gamma^* q \to qq\bar{q}$ remain equal for

$\sqrt{s} \geqq 100\,\text{GeV}$. One notices a α_s-hierarchy of cross-sections, namely $\sigma_{\text{total}} > \sigma_{3\text{-jet}}(\alpha_s) > \sigma_{4\text{-jet}}(\alpha_s^2)$.

In Figs. 8–10 we finally show the dependences of the various cross-sections on the basic kinematical variables x, y and W^2. (We do not show the Q^2-dependence since the Q^2-dependence is dominated by the $1/Q^2$-behaviour coming from the photon propagator). The x distribution of the cross-sections, Fig. 8, is mainly governed by the respective parton densities. Recalling that the lower limit of the momentum fraction of the incoming parton η increases with x (see (91)) it is clear that the gluon initiated processes dominate over the quark initiated cross-sections both in $O(\alpha_s)$ and in $O(\alpha_s^2)$ at low and high values of x. The same pattern is found in the comparison of the three-quark final state and the one quark-two gluons final state of the quark initiated cross-sections. Due to the specific way that these $O(\alpha_s^2)$ processes couple to the photon and the proton the three-quark final state probes more of the sea contributions whereas the one quark-two gluons final state probes more of the valence contributions in the proton.

The y distributions Fig. 9 are similar for all processes. There is a steep fall-off at low y values and a rather flat behaviour for y larger than $y \cong 0.04$. In particular there is no cross-over of the various processes. The W distributions in Fig. 10, on the other hand, again show the cross-over of the quark and gluon initiated processes at low W. This is a reflection of the x-behaviour since $W^2 = (1-x)ys$. However, it is interesting to observe that both the $O(\alpha_s)$ and the $O(\alpha_s^2)$ distributions decrease faster than the distribution of the total cross-section as the hadronic mass W increases. Thus, contrary to naive expectation, the 3-jet and 4-jet rates actually decrease as there is more energy available in the hadronic system. This can be traced back to the invariant mass cut condition (89) where we demanded that the jet-jet separation increases with increasing W. Since the choice of the mass scale in (89) is not unique it will be interesting to experimentally test the W-dependence of the jet rates. Such measurements should allow one to pin down the uncertainty in the description of QCD jets in DIS scattering with its (unique) feature of possessing more than one mass scale, e.g. Q^2 and W^2 or $p_\perp^2$.

6 Summary

In this paper we have evaluated the helicity amplitudes of all tree graph parton subprocesses contributing to deep inelastic ep scattering in $O(\alpha_s^2)$. All partons were assumed to be massless. Using new helicity techniques together with clever gauge choices we obtained concise expressions for the various $O(\alpha_s^2)$ tree graph amplitudes, $q + \text{boson} \to q + g + g$, $q + \text{boson} \to q + q' + \bar{q}'$ and $g + \text{boson} \to q + \bar{q} + g$. We have written down the necessary colour, flavour and statistical factors that are needed to compute the partonic hard scattering cross-sections from the helicity amplitudes. We explicitly stated the electroweak coupling terms and specified how the partonic cross-sections are folded with the respective parton densities to obtain the ep jet cross-sections of $O(\alpha_s^2)$.

We developed an efficient numerical Monte Carlo 4-jet routine which was used to study the various $O(\alpha_s^2)$ 4-jet processes where we limited our discussion to the one-photon exchange case. The DIS region was defined by suitable cuts in x, Q^2 and W^2. To obtain finite tree graph cross-sections the IR/M singular regions of the phase space have to be excluded. We introduced invariant mass cuts and discussed their choice in great detail. Contrary to the e^+e^- case there is no fixed reference mass scale for jet definition. A particular feature in ep collisions, as compared to $p\bar{p}$ collisions, is the presence of different, a priori equally important, mass scales. We elaborated on the implications of the nonexistence of an unique mass scale that can be used for jet definitions at ep colliders. For comparison we also considered the $O(\alpha_s)$ processes as well as the total DIS cross-section. Finally we presented differential distributions in basic kinematical variables. They allow for a separation of the various $O(\alpha_s^2)$ subprocesses. Somewhat surprisingly we found that both the 3-jet and the 4-jet rates decrease with increasing total hadronic energy W. Since this is a remnant of the chosen jet definition scheme it will be interesting to test it experimentally. The freedom in the choice of different mass scales has to be pinned down before one can try to extract the strong coupling constant α_s, or observe its Q^2-dependence.

The characteristic behaviour of the 3-jet and 4-jet rates with e.g. W is also important for background calculations. Here one usually relies on parton cascade (PC) models. Yet the uncertainty in the choice of a mass scale inherent in these models, in particular in DIS ep collisions, becomes relevant for multi-jet production. For example in the program LEPTO [7] the jet multiplicity increases with W when taking W as preferred mass scale. Thus multi-jet final states will be overestimated. With fixed order calculations at hand it will become possible to tune the PC models so that they reproduce the predictions of perturbative QCD, at least for low jet multiplicities.

While we were completing this work we received two papers on the subject of helicity amplitudes relevant to four-jet production in DIS [27, 26].

References

1. M. Bengtsson, G. Ingelman T. Sjöstrand; DESY preprint, DESY 87-097 (1987); Nucl. Phys. B301 (1988) 554
2. W. Furmanski, R. Petronzio: Z. Phys. C—Particles and Fields 11 (1982) 293
3. A. Mendez: Nucl. Phys. B145 (1978) 199
4. R.D. Peccei, R. Rückl: Nucl. Phys. B162 (1980) 125
5. J.G. Körner, E. Mirkes, G. Schuler: Int. J. Mod. Phys. A4 (1989) 1781

6. M. Bengtsson, T. Sjöstrand, M. van Zijl: Z. Phys. C—Particles and Fields 32 (1986) 67
7. G. Ingelman: LEPTO 4.3, CERN program pool W5046 (1986); LEPTO 5.2, DESY preprint in preparation
8. H.R. Wilson: Phys. Lett. 201B (1988) 361; Nucl. Phys. B310 (1988) 589
9. P. de Causmaecker, R. Gastmans, W. Troost, T.T. Wu: Phys. Lett. 105B (1981) 215; Nucl. Phys. B206 (1982) 53
10. F.A. Berends et al.: Phys. Lett. 103B (1981) 124
11. F.A. Berends et al.: Nucl. Phys. B206 (1982) 61
12. L. Chang, Z. Xu, D.H. Zhang: Nucl. Phys. B291 (1987) 392
13. G.R. Farrar, F. Neri: Phys. Lett. 130B (1983) 109
14. A. Kersch, F. Scheck: Nucl. Phys. B263 (1986) 475
15. F.A. Berends, W.T. Giele: Nucl. Phys. B294 (1987) 700
16. L. Clavelli, G.v. Gehlen: Phys. Rev. D27 (1983) 1495
17. T. Brodkorb, J.G. Körner, E. Mirkes: Phys. Lett. B216 (1989) 203
18. J.F. Gunion, Z. Kunzt: Phys. Lett. B159 (1985) 167
19. E. Byckling, K. Kajantie: Particle kinematics, London, New York, Sidney, Toronto Wiley 1973
20. A. Ali et al.: Nucl. Phys. B167 (1980) 454
21. J.G. Körner, G. Schierholz, J. Willrodt: Nucl. Phys. B185 (1981) 365
22. E. Eichten, I. Hinchliffe, K. Lane, C. Quigg: Rev. Mod. Phys. 56 (1984) 579; ibid. 58 (1986) 1047
23. P.N. Burrows, G. Ingelman, E. Ros: Z. Phys. C—Particles and Fields 39 (1988) 257
24. G.P. Lepage: CLNS-80/447 (1980) preprint
25. J.H. Friedman, M.H. Wright: CGTM-193-Rev. (1981); DIVON4, CERN program pool D151 (1981)
26. K. Hagiwara, D. Zeppenfeld: Nucl. Phys. B313 (1989) 560
27. F.A. Berends, W.T. Giele, H. Kuijf: Nucl. Phys. B321 (1989) 39